Design of Modulated and Demodulated Controllers for Flexible Structures [*]

K. Lau [1]   D. E. Quevedo   B. J. G. Vautier   G. C. Goodwin
S. O. R. Moheimani

School of Electrical Engineering & Computer Science,
The University of Newcastle,
Callaghan, NSW 2308, Australia

Abstract

We propose a novel method for controlling vibrations within a resonant structure equipped with piezoelectric transducers. The scheme uses a parallel connection of modulated and demodulated controllers, each designed to damp the transient oscillation corresponding to a single mode. This technique allows multiple modes to be controlled with a single actuator. A simulation example is presented and design considerations for the scheme are discussed. Experimental results obtained from a piezoelectric laminate cantilever beam confirm the theoretical analysis.

Key words: amplitude modulation, vibration control, active control, design issues

1   Introduction

There has been significant research interest in utilising piezoelectric transducers for vibration mitigation in resonant mechanical structures, see e.g. Moheimani and Goodwin (2001); Moheimani (2003); Fuller *et al.* (1996); Clark *et al.* (1998); Moheimani *et al.* (2003). By bonding piezoelectric materials to the surface of a resonant structure, these transducers can be used for vibration control, where they can be deployed as actuators, as sensors or both. For that purpose, several control algorithms have been proposed, see e.g. Hagood *et al.* (1990); Lazarus *et al.* (1991); Hagood and von Flotov (1991); Moheimani *et al.* (2001).

[1] Corresponding author, e-mail: K.Lau@newcastle.edu.au, Fax: +61 2 49601712

Given the fact that piezoelectric transducers can be accurately described with linear models over a significant operating range (Moheimani, 2000), both active and passive LTI (linear time invariant) methods have been proposed, see e.g. the survey in Moheimani (2003). Restricting controllers to be LTI is certainly attractive since, in this case, the design problem can be cast in the well studied LTI control systems framework, see e.g. Goodwin *et al.* (2001). On the other hand, it is well known that resonant systems are not always easy to control with LTI methods (Serón *et al.*, 1997; Goodwin *et al.*, 2001). As a consequence, depending upon the application, non-LTI methods may be worth studying, see e.g. Corr and Clark (2003) for work on nonlinear switching methods within this context.

In the present work, we propose a time varying (more precisely, periodic) vibration control method for resonant systems. It makes use of the fact that signals within a resonant structure are of an oscillatory nature, and hence concentrate their energies around a set of discrete frequencies, which correspond to the modes of the mechanical system. The method described here utilises concepts from amplitude-modulated communication systems in order to isolate and shift the spectrum of the high-frequency oscillations down to the *baseband*. It then operates on these low frequency signals. This corresponds to controlling the envelope of the oscillations and has strong conceptual and computational advantages, when compared to operating on high frequency signals.

Our methodology is based upon so-called *modulated* and *demodulated* control methods, which have been proven to be effective in a number of applications, see e.g. Bode (1945); Chen *et al.* (2005); Chang (1993); Leland (2001); Gerber (1978). Specifically, in relation to vibration suppression of flexible structures, an indirect method has been proposed in Chang (1993). It utilises the plant output as the modulation signal which translates energy into the baseband. The method emulates modulation with exogenous signals by relying upon a, rather *ad-hoc*, non-linear gain adjust module. Implicit in Chang (1993) is the assumption that the controlled plant output always has enough energy at the natural frequencies of the structure so as to provide an adequate modulation signal. This certainly constitutes a limiting factor, since the aim of the controller resides precisely in vibration suppression.

As shown by Chang (1993), one of the advantages of using modulation and demodulation is that it allows the modes of the structure to be controlled using a low bandwidth controller. This is particularly useful in the control of high frequency vibration modes.

In the present paper, we propose to utilise modulated and demodulated control with exogenous modulation signals. This allows one to control several modes with a single piezoelectric actuator in a simple manner. It also overcomes the

above mentioned limitations of the output-modulation based method of Chang (1993). We study the behaviour of the resulting closed loop system using several linear models each of which yields different insights. Indeed, the closed loop behaviour turns out to be governed by a trade-off between attenuation and stability margin.

Our work extends Lau *et al.* (2004*b*) to the control of multiple modes within a resonant structure, which we assume fixed and known. Preliminary ideas can also be found in our conference contribution (Lau *et al.*, 2004*a*).

The remainder of the paper is organised as follows: In the next section, we describe the system to be controlled. Then, in Section 3, we investigate the application of modulated control to vibration damping. Section 4 elucidates design considerations, and Section 5 documents experimental studies. Section 6 concludes the paper.

2   Piezoelectric Beam Model

Piezoelectric materials can transform electrical energy into mechanical energy and *vice versa*. Thus they can be deployed as actuators, as sensors or both. More precisely, due to their permanent dipole nature, piezoelectric materials strain when exposed to an electric field and conversely produce an electric charge when strained. More details can be found e.g. in Fuller *et al.* (1996); Moheimani (2003).

In the present work, we concentrate upon the piezoelectric laminate beam schematised in Fig. 1. In this configuration, the beam is fixed at one end and free at the other. Three piezoelectric patches are mounted on the beam, two being collocated. As shown in Fig. 1, one patch is used as an actuator, i.e., it transforms the voltage $u(t)$ into strain. Another patch functions as a sensor, providing a voltage $v(t)$, which depends upon the (local) beam deflection. The beam is also equipped with a piezoelectric actuator, which represents disturbances. Despite the fact that often disturbances on a flexible structure are of a distributed nature, from an experimental viewpoint, it is convenient to utilise a lumped model where the disturbance, denoted here as $d_o(t)$, exerts a moment on the beam.

The overall goal of our work is to provide a controller for the system depicted in Fig. 1 which, based upon the measured signal $v(t)$ and by manipulating the signal $u(t)$, mitigates the vibration caused by $d_o(t)$. We also examine the displacement $z(t)$, which corresponds to some other point Z on the beam.

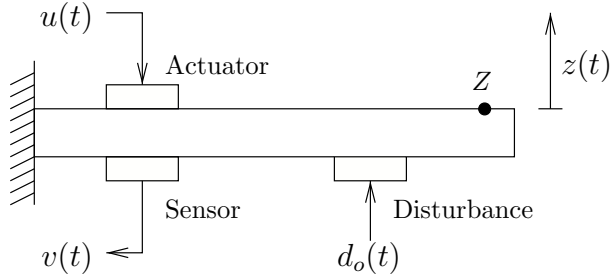The laminate beam of Fig. 1 is governed by a partial differential equation

Fig. 1. Piezoelectric laminate beam.

which can be solved in a variety of ways, see e.g. Fuller *et al.* (1996); Pota *et al.* (1999); Moheimani *et al.* (2003). In the present work, we will utilise the following model, taken from Moheimani (2003):

$$
\begin{aligned}
v(t) &= G_{vu}(s)u(t) + G_{vd}(s)d_o(t) \\
z(t) &= G_{zu}(s)u(t) + G_{zd}(s)d_o(t).
\end{aligned}
\tag{1}
$$

Here, $G_{vu}(s)$, $G_{vd}(s)$, $G_{zu}(s)$ and $G_{zd}(s)$ are linear time invariant transfer functions, which reflect the resonant nature of the beam. In principle, they contain an infinite number of natural modes, being of the form

$$
\sum_{i=1}^{\infty} \frac{\gamma_i}{s^2 + 2\zeta_i\omega_i s + \omega_i^2},
\tag{2}
$$

where ω_i are the resonance frequencies and ζ_i are their (uncontrolled) damping factors. The scalars γ_i depend upon the position of the piezoelectric patches and, in the collocated case of Fig. 1, are always non-negative.

For control design purposes it is convenient to truncate the model structure (2) such that only M modes are considered. Thus, the relationship between $u(t)$ and $v(t)$ can be described as:

$$
G_{vu}(s) = D + \sum_{i=1}^{M} \frac{\gamma_i}{s^2 + 2\zeta_i\omega_i s + \omega_i^2},
\tag{3}
$$

where the scalar D accounts for the spillover effect of the neglected terms over the bandwidth of interest (Clark, 1997; Moheimani, 2000). The transfer functions $G_{vd}(s)$, $G_{zu}(s)$ and $G_{zd}(s)$ are commonly of the same form as $G_{vu}(s)$ and often only differ in the location of their zeros, i.e. in the values adopted by the terms γ_i and D in (3).

3   The Proposed Controller Architecture

As stated above, we will use feedback from the sensor signal $v(t)$ to the actuator signal $u(t)$ to suppress vibrations in the beam. The controller consists

4

of a parallel connection of systems, each designed to damp a single mode. For ease of exposition, we will first consider the control of a single mode and then describe the multimodal architecture.

3.1 Notation

Arg z denotes the principal argument of z. Thus $-\pi < \text{Arg}\, z \leq \pi$. A symbol with a tilde denotes a modulated signal. If $\tilde{f} = f(t)\cos\omega t$ then we refer to f as the envelope of $\tilde{f}$. Important exceptions to this rule are the system inputs and outputs u, v, d_o and z. Upper case denotes the Laplace transform of a signal. In the sequel, $G(s)$ and $G_{vu}(s)$ are used interchangeably.

3.2 Control of a Single Mode

The control scheme for a single mode (at frequency ω_i) is depicted in Fig. 2. In this figure, $G(s) = G_{vu}(s)$, and $\tilde{d}(t)$ is an output disturbance which can be used to model initial conditions as well as the effect of $d_o(t)$. The single-mode controller has two branches, each consisting of a demodulator, an LTI controller $C_i(s)$ (the *baseband controller*), and a modulator. Within each branch, $v(t)$ is first demodulated by correlating it with $\cos(\omega_i t + \phi)$ (or $\sin(\omega_i t + \phi)$) and then filtered by a low-pass filter $F_i(s)$. Each demodulated signal is then passed through $C_i(s)$ and the resulting signal is used to modulate $\cos\omega_i t$ (or $\sin\omega_i t$). We note that the two demodulators (and the two modulators) are $\pi/2$ rad out of phase, and hence they are orthogonal. The phase shift ϕ_i is defined as $\text{Arg}[G(j\omega_i)]$ and may be approximated by $-\pi/2$.
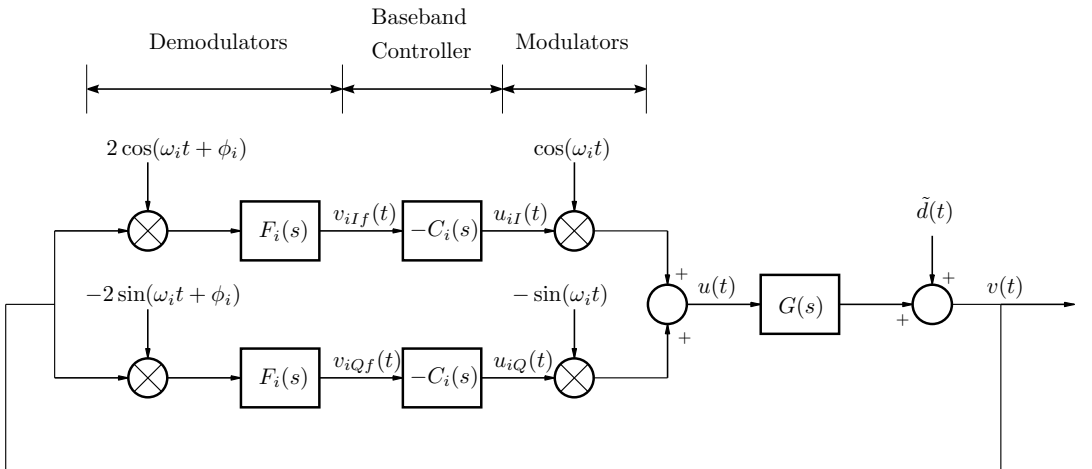

Fig. 2. Single mode control scheme.

5

Since we are dealing with resonant structures governed by (2), the sensor output $v(t)$, has its energy concentrated in narrow bands centred about the resonance frequencies of the system. Thus, $v(t)$ can be written as a sum of modulated signals, i.e.,

$$v(t) = \sum_{k=1}^{\infty} \tilde{v}_k(t), \tag{4}$$

where

$$\tilde{v}_k(t) = v_{kI}(t)\cos(\omega_k t + \phi_k) - v_{kQ}(t)\sin(\omega_k t + \phi_k), \tag{5}$$

and $v_{kI}(t)$ and $v_{kQ}(t)$ are band-limited (low-pass) signals with bandwidths $\leq \Omega_k$ (i.e., $|V_{kI}(j\omega)|$ and $|V_{kQ}(j\omega)|$ are small for $\omega > \Omega_k$). We refer to the the cos and sin terms in (5) as the in-phase and quadrature components of $\tilde{v}_k(t)$. We note that $v_{kI}(t)$ and $v_{kQ}(t)$ are the envelopes of these components.

It can be seen that

$$2\tilde{v}_i(t)\cos(\omega_i t + \phi_i) = v_{iI}(t)[1 + \cos(2(\omega_i t + \phi_i))] - v_{iQ}(t)\sin(2(\omega_i t + \phi_i)).$$

Moreover, for $k \neq i$, $2\tilde{v}_k(t)\cos(\omega_i t + \phi_i)$ has its energy concentrated in narrow bands centred at $\omega_i \pm \omega_k$ and $-\omega_i \pm \omega_k$. It follows that $v_{iIf}(t)$ is $v_{iI}(t)$ filtered by $F_i(s)$ provided that the following assumptions are satisfied:

Assumptions

A1. $\omega_i > \Omega_i$ and $|\omega_i - \omega_k| > \Omega_i + \Omega_k$ for all $k \neq i$.
A2. $F_i(s)$ is a low-pass filter with bandwidth Ω_i, i.e., $|F_i(j\omega)| \approx 0 \ \forall \ \omega > \Omega_i$.

In a similar manner, it can be shown that, if A1 and A2 hold, then $v_{iQf}(t)$ is approximately equal to $v_{iQ}(t)$ filtered by $F_i(s)$.

The baseband controllers transform the filtered envelopes $v_{iIf}(t)$ and $v_{iQf}(t)$ to produce $u_{iI}(t)$ and $u_{iQ}(t)$, the envelopes of the in-phase and quadrature components of $u(t)$. We note that the phases of the modulators and demodulators are chosen so that the two input two output (TITO) system from $\mathbf{u_i} = [u_{iI}, \ u_{iQ}]^T$ to $\mathbf{v_{if}} = [v_{iIf}, \ v_{iQf}]^T$ is 'decoupled (diagonal) at dc'. Hence, it is reasonable to use $u_{iI}(t)$ to control the in-phase component of $\tilde{v}_i(t)$ and $u_{iQ}(t)$ to control the quadrature component.

3.3   Multimodal Modulated Control

Multiple, say M_c, modes can be controlled in a decentralised manner by using one modulated controller per mode. This is illustrated in Fig. 3 for the case of a two mode controller, i.e., $M_c = 2$. In this figure, $\mathscr{C}_i$ denotes the controller for the ith mode (see Fig. 2), and $\tilde{u}_i(t) = u_{iI}(t)\cos\omega_i t - u_{iQ}(t)\sin\omega_i t$. It is

worthwhile to note that each of the single mode controllers acts as a band-pass filter (this is shown in Section 4.1 below). It follows that the multimodal scheme is, at least conceptually, similar to filter banks which are widespread in signal processing applications, see e.g. Vaidyanathan (1993).
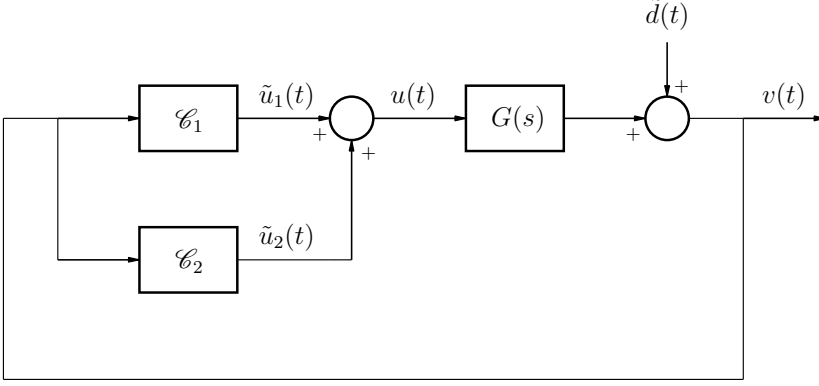

Fig. 3. Multimodal control scheme for two modes.

We emphasise that when controlling M_c modes, an underlying assumption of the scheme is that the closed loop output $v(t)$ satisfies (compare to (4))

$$v(t) = \sum_{k=1}^{M_c} \left(v_{kI}(t) \cos(\omega_k t + \phi_k) - v_{kQ}(t) \sin(\omega_k t + \phi_k) \right),$$

where $v_{kI}(t)$ and $v_{kQ}(t)$ are band-limited signals. It is also assumed that $u_{kI}(t)$ and $u_{kQ}(t)$ are band-limited. Let Ω_k be an upper bound on the bandwidths of these signals. We require that $F_i(s)$ and Ω_i satisfy the following conditions:

C1. $\Omega_1 < \omega_1$ and $\Omega_i + \Omega_{i+1} < \omega_{i+1} - \omega_i$ for $i = 1, 2, .., M_c - 1$.
C2. $F_i(s)$ is a low-pass filter which rolls off for $\omega > \Omega_i$.
C3. $|F_i(j(\omega_k - \omega_i))G(j\omega_k)| \ll |F_i(0)G(j\omega_i)|$, $i \neq k$.

These conditions ensure that the coupling between the modes is relatively small. In particular, the third condition implies that, for $i \neq k$, the gain from $\mathbf{u_i}(t)$ to $\mathbf{v_{kf}}(t)$ (or, equivalently, the gain from $\tilde{u}_i(t)$ to $\tilde{v}_k(t)$) is small. The conditions also ensure that the baseband approximation (given below in Lemma 1 of Section 4.1) can be applied.

As outlined above, the modes can be considered to be approximately decoupled, and hence the corresponding controllers designed independently.

7

4 Design Considerations

4.1 Linear Analysis of the Control Scheme

The scheme in Fig. 2 is clearly time-varying (periodic), and is, thus, in principle, difficult to analyse. However, approximately equivalent LTI systems may be found. We will consider two alternative approaches. The first gives a TITO approximate (baseband) model. When further simplified to a pair of decoupled SISO systems, this gives deep insights into the controller design. The second (narrowband) approach is exact and gives a quantification of stability margins etc., but is slightly less insightful.

The baseband approach approximates the TITO system from $\mathbf{u_i}$ to $\mathbf{v_{if}}$ by a linear system with transfer function $G_{2\times 2}(s, \omega_i)$, as shown in Fig. 4. In this figure, $\mathbf{d_{if}}(t) = [d_{iIf}(t), d_{iQf}(t)]^T$ is the demodulated disturbance. As will be discussed in this section, the TITO baseband model can be further approximated by a pair of decoupled SISO baseband models.

Remark 1 *We note that, in practice, the low-pass filter $F_i(s)$ may introduce a significant delay (relative to $1/\omega_i$) into the system. This would seem to imply that it is difficult to control the system at ω_i rad/s. However, it is clear from Fig. 4 that the filter delay limits only the speed of response of the baseband system, not the full system. Thus, the delay limits only the speed of response of the* envelope of $\tilde{v}_i$. *This fact is analysed in more detail in Lau* et al. *(2004b).*
□

The narrowband approach replaces the controller (from $v(t)$ to $u(t)$) by an exact transfer function $C_{im}(s)$. The resulting closed loop system is shown in Fig. 5.

The following lemma gives the expression for the TITO transfer function $G_{2\times 2}(s, \omega_i)$ in the baseband model shown in Fig. 4.

Lemma 1 *Consider the system in Fig. 2. Suppose that $u_{iI}, u_{iQ}, v_{iI}, v_{iQ}$ are band-limited with bandwidths $\leq \Omega_i$, where $\Omega_i < \omega_i$, and $F_i(s)$ is a low-pass filter with bandwidth Ω_i. Then the system from $[U_{iI}(s), U_{iQ}(s)]^T$ to $[V_{iIf}(s), V_{iQf}(s)]^T$ can be approximated by a linear system with transfer function $G_{2\times 2}(s, \omega_i)F_i(s)$ (as shown in Fig. 4), where*

$$G_{2\times 2}(s, \omega_i) = \begin{bmatrix} G_m(s, \omega_i) & G_x(s, \omega_i) \\ -G_x(s, \omega_i) & G_m(s, \omega_i) \end{bmatrix},$$

$$G_m(s, \omega_i) = \frac{1}{2} \left[e^{-j\phi_i} G(s + j\omega_i) + e^{j\phi_i} G(s - j\omega_i) \right]$$

$$\text{and} \quad G_x(s, \omega_i) = \frac{j}{2} \left[e^{-j\phi_i} G(s + j\omega_i) - e^{j\phi_i} G(s - j\omega_i) \right].$$

Proof
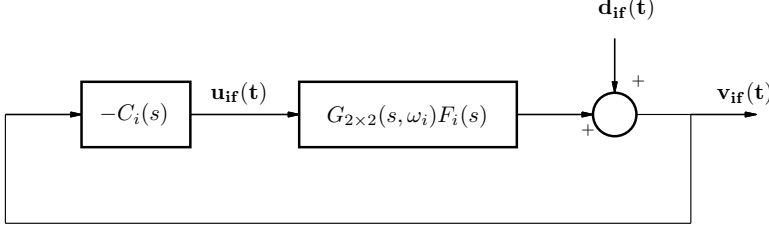
See Appendix A.1. □

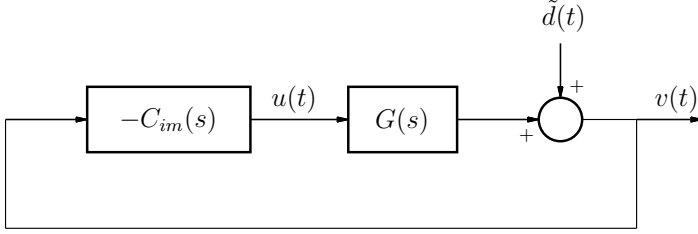Fig. 4. Equivalent (TITO) baseband system.

Fig. 5. Equivalent narrowband system.

Remark 2 *It can be seen that $G_x(0, \omega_i) = 0$. By continuity, this implies that, for small ω, $G_{2\times2}(j\omega, \omega_i)$ can be approximated by $G_m(j\omega, \omega_i)I_2$, where I_2 is the 2×2 matrix identity. For this reason, we refer to this approximation as the SISO baseband model, and we refer to $G_m(s, \omega_i)$ as the SISO baseband transfer function. Note that the SISO baseband model, by its very nature, does not describe the potential interactions that can arise between the in-phase and quadrature components.* □

It is useful to elucidate the properties of the SISO baseband transfer function $G_m(s, \omega_i)$. For that purpose, let $G(s) = N(s)/D(s)$, where $N(s)$ and $D(s)$ are coprime polynomials. Then

$$G_m(s, \omega_i) = \frac{1}{2} \frac{N_m(s, \omega_i)}{D_m(s, \omega_i)}, \tag{6}$$

where

$$N_m(s, \omega_i) = e^{-j\phi_i} N(s + j\omega_i) D(s - j\omega_i) + e^{j\phi_i} N(s - j\omega_i) D(s + j\omega_i), \tag{7}$$

9

and
$$D_m(s, \omega_i) = D(s + j\omega_i)D(s - j\omega_i). \tag{8}$$

We refer to the zeros of $N_m(s, \omega_i)$ as the *zeros* of $G_m(s, \omega_i)$ and the zeros of $D_m(s, \omega_i)$ as the *poles* of $G_m(s, \omega_i)$. Thus, $G_m(s, \omega_i)$ may contain pole zero cancellations.

It can be shown that $G_m(s, \omega_i)$ has the following properties (Lau *et al.*, 2004*b*, Lemmata 5.1, 5.6, 5.7):

Property 1 The poles of $G_m(s, \omega_i)$ are the poles of $G(s)$ shifted by $j\omega_i$ and $-j\omega_i$.

Property 2 If $G(s)$ has poles at $p \in \mathbb{C}$ and $p + 2j\omega_i$, then $G_m(s, \omega_i)$ has two poles and one zero at $p + j\omega_i$.

Property 3 If $G'(s) = e^{-s\tau}G(s), \tau > 0$, then $G'_m(s, \omega_i) = e^{-s\tau}G_m(s, \omega_i)$.

Remark 3 *If $G(s)$ has a pair of poles at $a \pm j\omega_i$, then $G_m(s, \omega_i)$ has a double pole at a and a pair of poles at $a \pm 2j\omega_i$ (Property 1). $G_m(s, \omega_i)$ also has a zero at a which cancels one of the poles (Property 2). If $\omega_0 \approx \omega_i$, then $G_m(s, \omega_0)$ contains an approximate cancellation.* □

The next lemma provides an expression for $C_{im}(s)$ in the narrowband model shown in Fig. 5. We note that this result has been proved previously (for the special case of $F_i(s)C_i(s) = 1/s$ in Bodson *et al.* (1994).

Lemma 2 *Let $(FC)_i(s)$ denote $F_i(s)C_i(s)$. Then the modulated and demodulated controller in Fig. 2 has the following transfer function:*

$$-C_{im}(s) = -\left[e^{-j\phi_i}(FC)_i(s - j\omega_i) + e^{j\phi_i}(FC)_i(s + j\omega_i) \right].$$

Proof

See Appendix A.2. □

Remark 4 *Suppose that $C_i(s)$ is a constant gain. Then from Lemma 2, it can be seen that the modulators and demodulators convert the low-pass filter $(FC)_i(s)$ to a band-pass filter.* □

In the above development, we have described two alternative approaches for the analysis of the scheme in Fig. 2. These two approaches yield three alternative models. Specifically, the application of Lemma 1 yields the TITO baseband model shown in Fig. 4, which can be further simplified (when s is small) to a SISO baseband model. Alternatively, the application of Lemma 2 yields the narrowband model shown in Fig. 5. A comparison of the methods/models will be given in Sections 4.3 and 4.4.

Let $L_i(s)$, $L_{ia}(s)$ and $\tilde{L}_i(s)$ denote the loop transfer functions of the TITO baseband model, the SISO baseband model and the narrowband model, re-

spectively. We note that

$$L_{ia}(s) = G_m(s, \omega_i)F_i(s)C_i(s)$$
$$= \frac{1}{2} \left[e^{-j\phi_i}G(s + j\omega_i) + e^{j\phi_i}G(s - j\omega_i) \right] (FC)_i(s),$$

and that

$$\tilde{L}_i(s) = G(s)C_{im}(s)$$
$$= G(s) \left[e^{-j\phi_i}(FC)_i(s - j\omega_i) + e^{j\phi_i}(FC)_i(s + j\omega_i) \right].$$

It can easily be shown that, when $|s|$ is small, $L_{ia}(s)$ and $\tilde{L}_i(s)$ are related as follows:

$$L_{ia}(s) \approx \frac{1}{2} \left[\tilde{L}_i(s + j\omega_i) + \tilde{L}_i(s - j\omega_i) \right].$$

We also note that the loop gain at the ith mode, $\tilde{L}_i(j\omega_i)$, is approximately equal to $L_{ia}(0) = |G(j\omega_i)|(FC)_i(0)$.

For the multimodal scheme, the loop transfer function for the entire system (narrowband approach) is given by

$$\tilde{L}(s) = \sum_{i=1}^{M_c} \tilde{L}_i(s), \tag{9}$$

and the closed loop transfer function from $D_o(s)$ to $Z(s)$ is given by

$$T_{zd}(s) = G_{zd}(s) - \frac{G_{zu}(s)G_{vd}(s)}{G_{vu}(s)} \frac{\tilde{L}(s)}{1 + \tilde{L}(s)}.$$

These relations will be used in the controller design as described below.

4.2 Simulation Example

In this section, we illustrate the principles outlined above by applying the modulated controller to a simplified two-mode model of a beam. This example provides insight into the scheme, in particular, into the relationship between the baseband and narrowband models developed in the previous section.

We give simulation results for the control of the flexible beam modelled in Pota *et al.* (1999). The beam is 0.775 m long and 0.05 m wide, and can be modelled by (3) with $D = 0$, $M = 2$, $\gamma_1 = 32.29$, $\gamma_2 = 584.39$, $\zeta_1 = \zeta_2 = 0.008$, $\omega_1 = 50.18$ rad/s and $\omega_2 = 314.46$ rad/s. The model $G_{vu}(s)$ has poles at approximately [2] $-a_1 \pm j\omega_1$ and $-a_2 \pm j\omega_2$, where $a_1 \approx 0.4$ and $a_2 \approx 2.52$.

---

[2] The imaginary parts of the poles are actually $\pm\sqrt{1 - \zeta_i^2}\omega_i \approx \pm\omega_i$.

It follows that the time constant of the (envelope of) the first mode is $1/0.4$ s and that of the second mode is $1/2.52$ s.

In this example, we use the SISO baseband model to design the controller. We recall that the use of this model reduces the control problem to one of choosing $C_i(s)$ to control $G_m(s, \omega_i)F_i(s)$. As noted in Remark 3, $G_m(s, \omega_1)$ has a pair of poles and a zero at approximately $-a_1$. It follows that $G_m(s, \omega_1)$ contains an approximate pole zero cancellation at $-a_1$. Since the rest of the poles are large, $G_m(s, \omega_1)$ has a dominant pole at $-a_1$. Similarly, $G_m(s, \omega_2)$ has a dominant pole at $-a_2$. We note that the transient response (of $G_m(s, \omega_i)$) associated with a_i corresponds to the envelope of the ith mode of $G_{vu}(s)$.

We take $F_1(s)$ and $F_2(s)$ as fourth order Butterworth filters with bandwidths $\Omega_1 = 20$ and $\Omega_2 = 50$, respectively, to satisfy the conditions given in Section 3.3. The Bode magnitude plots of $G_{vu}(s)F_1(s - j\omega_1)$ and $G_{vu}(s)F_2(s - j\omega_2)$ are shown in Figs. 6 and 7, respectively. From these diagrams, it is clear that $F_1(s - j\omega_1)$ and $F_2(s - j\omega_2)$ have strong attenuation at $s = j\omega_2$ and $s = j\omega_1$, respectively.
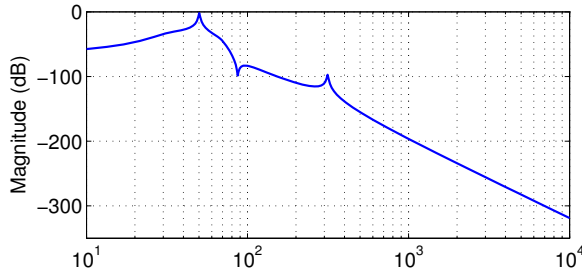

Fig. 6. Bode magnitude plot of $G_{vu}(s)F_1(s - j\omega_1)$ showing the attenuation of the peak at the second mode.
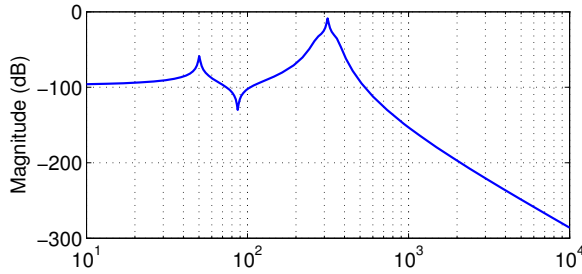

Fig. 7. Bode magnitude plot of $G_{vu}(s)F_2(s - j\omega_2)$ showing the attenuation of the peak at the first mode.

The upper plots in Figs. 8 and 9 show the transient uncontrolled responses $\tilde{v}_1(t)$ and $\tilde{v}_2(t)$. The lower plots in the figures show the controlled responses with $C_1(s) = C_2(s) = 5$ (i.e., proportional control in the baseband) and both of the loops closed. We observe that the closed loop responses are significantly faster than the open loop ones. Note that $C_1(s)$ shifts the dominant pole of $G_m(s, \omega_1)$ from $-a_1 \approx -0.4$ to -2.65. This is equivalent to shifting the poles of

$G_{vu}(s)$, corresponding to the first mode, to the left (increasing the damping). Similarly, $C_2(s)$ shifts the dominant pole of $G_m(s, \omega_2)$ from -2.52 to -10.33.
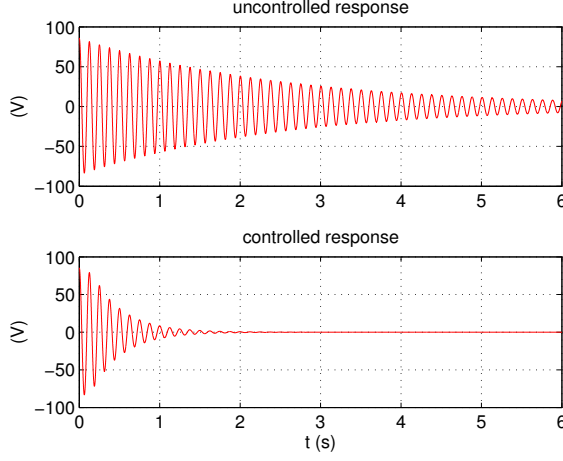

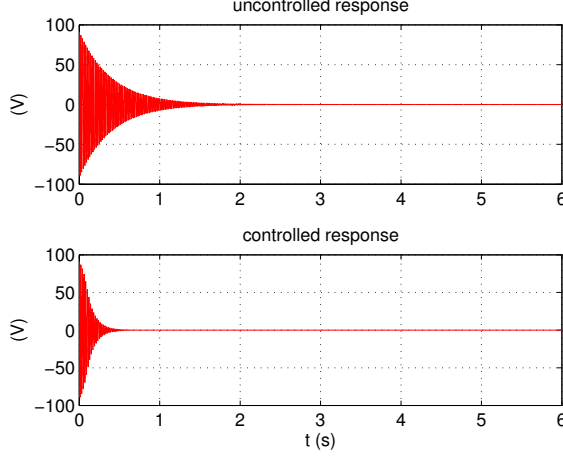Fig. 8. First mode time responses $(\tilde{v}_1(t))$.

Fig. 9. Second mode time responses $(\tilde{v}_2(t))$.

As discussed in Section 2, we are often interested in the vibration measured at another point on the beam. Fig. 10 contains plots of the displacement, $z(t)$, measured at a point 0.76 m from the fixed end. The open and closed loop responses are both shown. In this case, we have, $\gamma_{z1} = 0.0028$ and $\gamma_{z2} = -0.0013$ (Pota *et al.*, 1999). We note that the response is dominated by the first mode.

Let $d_u(t)$ be an additive input disturbance which enters the closed loop system at the input to $G_{vu}(s)$. Figs. 11 and 12 show the open and closed loop frequency response (magnitude only) from d_u to v and to z, respectively. The responses up to the third mode are shown. We note that the open loop responses were obtained by plotting $|G_{vu}(j\omega)|$ and $|G_{zu}(j\omega)|$. The closed loop responses were 'measured' by simulating the system in Fig. 3 with $G_{vu}(s)$ replaced by a three mode approximation to $G_{vu}(s)$. The initial conditions were set to zero ($\tilde{d}(t) =$
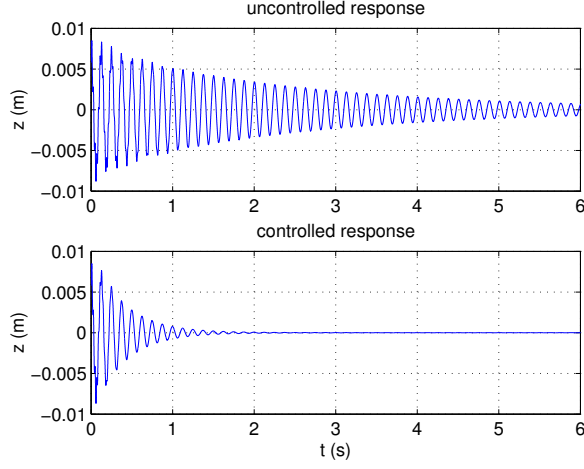
13

Fig. 10. Time responses for z.

0) and the frequency response estimated by injecting a series of sine waves at d_u. It can be seen that the controller attenuates the peak at the first and second mode by approximately 14 dB and 9 dB, respectively. These values are given by $1/(1 + G_m(0, \omega_i)C_i(0))$ for $i = 1, 2$. As one would expect, the third mode is essentially unaffected by the controller.
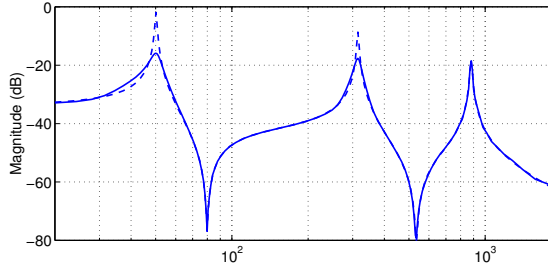

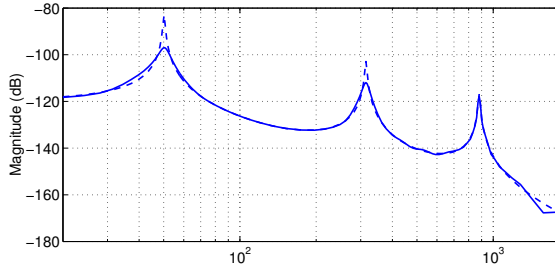Fig. 11. Open loop (dotted) and closed loop (solid) frequency responses (d_u to v).

Fig. 12. Open loop (dotted) and closed loop (solid) frequency responses (d_u to z).

Remark 5 *The simulations documented above were performed using the nominal plant $G_{vu}(s)$. However, we note that if we replace $G_{vu}(s)$ in the simulations by, for example, an eight mode approximation of $G_{vu}(s)$ then the time responses $\tilde{v}_1(t)$ and $\tilde{v}_2(t)$ turn out to be almost identical. This implies that the higher modes are sufficiently decoupled from the lower two so as not to affect the performance of the controller.* □

14

4.3 Baseband vs. Narrowband

In this section, we provide a brief discussion of the relative merits of the TITO baseband model, the SISO baseband model, and the narrowband model.

In the TITO baseband model, the modulated and demodulated plant is replaced by an equivalent TITO baseband system (i.e., the plant is shifted down to the baseband). This approach has benefits in the design of the baseband controller since $C_i(s)$ appears directly in the loop transfer function. The approach also allows one to use a non-diagonal TITO controller.

As we have illustrated in Section 4.2, the use of the simplified SISO baseband model allows the problem of controlling a single mode to be reduced to one of controlling a simple first order system. It should be noted that, whilst the SISO model is useful for predicting the response of the closed loop, it should not be used to analyse the stability margins of the loop[3]. This is due to the fact that the first order approximation holds only for ω close to zero. This will be discussed further in Section 4.4.

In the narrowband model, the modulated and demodulated controller is replaced by an equivalent narrowband system (i.e., the controller is shifted up to the passband). It is clear that the design of the controller is less intuitive in this case. However, the loop transfer function $\tilde{L}_i(s)$ given in (9) can be used to analyse the stability margin (of the ith loop). Moreover, since $\tilde{L}_i(s)$ is exact, the stability analysis will also be exact. The narrowband approach also allows the entire multimodal scheme to be analysed, since the loop transfer function $\tilde{L}(s)$ is simply the sum of the individual loop transfer functions $\tilde{L}_i(s)$.

4.4 Comments on the First Order Approximation (SISO baseband model)

The assumption that $G_{2\times2}(j\omega, \omega_i) \approx G_m(j\omega, \omega_i)I_2$, is equivalent to the assumption that $G_x(j\omega, \omega_i) \approx 0$. To gain insight into this, let us suppose that $G_x(j\omega, \omega_i) = 0$. Then

$$
\begin{aligned}
e^{-j\phi_i}G(j\omega + j\omega_i) &= e^{j\phi_i}G(j\omega - j\omega_i) \\
&= \overline{e^{-j\phi_i}G(j\omega_i - j\omega)}.
\end{aligned}
\tag{10}
$$

---

[3] If one wishes to analyse the stability margin in the baseband, it is necessary to consider the TITO baseband loop transfer function $L_i(s)$. However, since $G_{2\times2}(s, \omega_i)$ is an approximate transfer function, $L_i(s)$ is also approximate. For a more accurate analysis, the narrowband loop transfer function $\tilde{L}_i(s)$ should be used.

Let $H(s) = e^{-j\phi_i} G(s + j\omega_i)$. Then condition (10) is equivalent to $H(j\omega) = \overline{H(-j\omega)}$. It follows that $G_{2 \times 2}(j\omega, \omega_i) = G_m(j\omega, \omega_i)I_2$ if and only if $e^{-j\phi_i} G(j\omega)$ is conjugate symmetric about $\omega = \omega_i$.

The preceding discussion implies that the first order approximation does not hold when the asymmetry of $H(j\omega)$ is significant. Since $H(j\omega)$ will never be perfectly symmetric the approximation will, in general, be valid only for sufficiently small ω. We note that the feedthrough term D causes asymmetry, and hence the approximation is valid for a smaller range of frequencies when D is large.

The first order approximation also neglects the effect of the filter. The filter introduces a phase shift, and hence can affect the stability/robustness of the closed loop.

It can thus be seen that the first order approximation holds for ω close to zero in the baseband (or for ω close to ω_i in the passband). However, the approximation neglects the asymmetry of $G(j\omega)$ about $\omega = \omega_i$, and also the phase shift introduced by the filter. In practice these additional features will not affect the closed loop response in the vicinity of the modes but may affect the analysis of the stability margin or robustness of the loop.

4.5   Choice of decoupling filters

Several factors need to be considered when designing the decoupling filters. The bandwidth of the filter should be greater than that of the closed loop system. The filter should also provide sufficient attenuation to prevent the modes from interacting. A large phase shift in the passband of the filter is also undesirable as this reduces the gain margin of the system.

It is clear that increasing the controller gain increases the attenuation of the mode, and also increases the closed loop bandwidth. It follows that, in order to increase the gain, a filter with a higher bandwidth and faster roll off (higher order) is required. This will be accompanied by an increase in the phase shift in the passband and a decrease in the gain margin. It can thus be seen that there will be a limit to how far the gain can be increased.

5   Experimental Study

In order to further investigate properties of the proposed controller architecture, we carried out experiments on a physical beam in the Laboratory of

Dynamics and Control of Smart Structures at The University of Newcastle, Australia.

5.1   Testbed

The experimental set-up used is built around a cantilever beam of length 55 cm, which is equipped with piezoelectric patches, as depicted in Fig. 1. The output voltage of the *sensor patch* is passed through a high-impedance buffer to avoid low-frequency distortion in $v(t)$. The *disturbance patch* is located at the centre of the beam. It is driven by a voltage source, which generates a disturbance in the beam. Tip displacement (point Z in Fig. 1) was measured with a Polytec laser scanning vibrometer (PSV-300). Controllers were implemented with a dSPACE DS-1103 DSP board (sampling frequency 50 kHz) and corresponding anti-aliasing and reconstruction filters.

5.2   System Identification

For the purpose of identifying the beam, i.e., to obtain models $G_{vu}(s)$, $G_{vd}(s)$, $G_{zu}(s)$ and $G_{zd}(s)$ within the structure (3), we decided to work in the frequency domain. Chirp signals (from 5 to 250 Hz) were applied to $u(t)$ and $d_o(t)$, and $v(t)$ and $z(t)$ were measured. The input/output data so obtained was processed in real time by the Polytec software in order to provide all four frequency responses.

We considered the case of controlling the first two modes of the beam (the extension to other modes follows the same principles). Thus, we identified a fourth-order model, i.e., we chose $M = 2$ in (3). The system modes and damping factors (parameters ω_i and ζ_i in (3)) were characterised directly by measuring size and location of the peaks of the experimental frequency response plots. Then, the feedthrough terms D and the gains γ_i were determined according to an optimisation procedure. More precisely, we set up an optimisation problem which minimises the normalised least square difference between model and measured frequency response. It can be seen from the frequency responses of Fig. 13, that the identified transfer functions match closely the experimental data in the bandwidth covering the first two modes.

5.3   Controller Design

The design of the modulated and demodulated controller requires the choice of two low-pass filters, $F_1(s)$ and $F_2(s)$ and two controller transfer functions
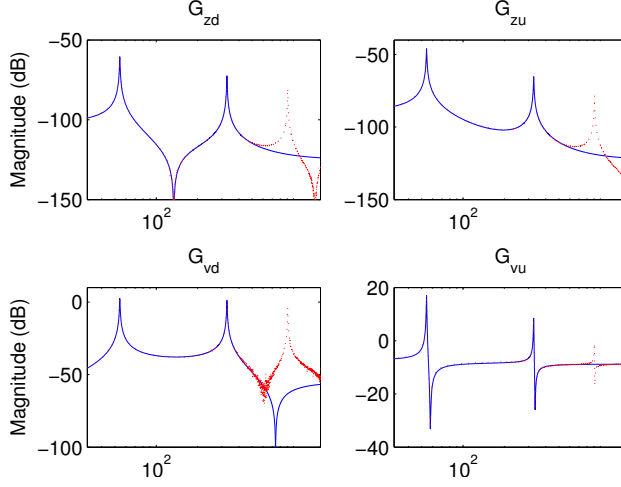
Fig. 13. Measured (dotted line) and model (solid line) frequency responses.

$C_1(s)$ and $C_2(s)$.

As in the simulation example (Section 4.2), we take $F_1(s)$ and $F_2(s)$ as fourth order Butterworth filters with bandwidths of $\Omega_1 = 20$ and $\Omega_2 = 50$, respectively. As it was found previously, these filters provide strong decoupling of the modes. It follows that $C_1(s)$ and $C_2(s)$ can be chosen independently. It has also been shown that the system can be controlled using proportional control in the baseband, and so, we let $C_1(s) = K_1$ and $C_2(s) = K_2$.

As a first guideline for tuning the two gains, we utilise the Nyquist plot of $G_{vu}(s)(C_{1m}(s) + C_{2m}(s))$ with $K_1 = K_2 = 1$ depicted in Fig. 14. From the Nyquist plot, it can be seen that the closed loop should be stable, if

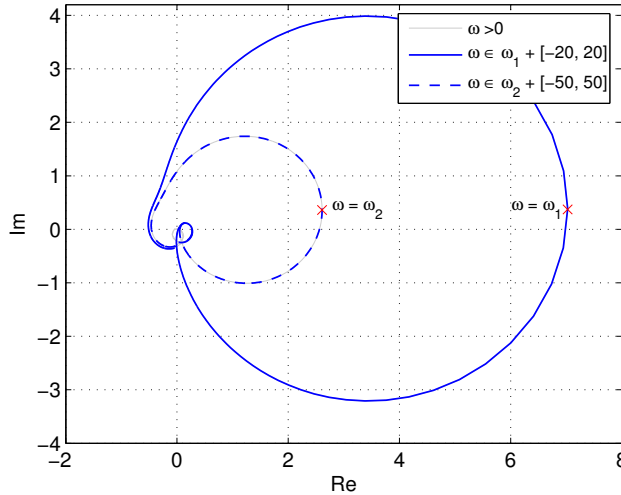$$K_1 \leq 1.96, \quad K_2 \leq 2.18. \tag{11}$$

Fig. 14. Nyquist plot of $G_{vu}(s)(C_{1m}(s) + C_{2m}(s))$ with $K_1 = K_2 = 1$ ($\omega > 0$ only).

The controller gains can also be chosen with the aid of the frequency responses shown in Figs. 15 and 16. These figures show the effect of K_1 and K_2 on $T_{zd}(j\omega)$, i.e., on the closed loop frequency response between disturbance $d_o(t)$ and displacement $z(t)$. We emphasise here, that K_1 does not have any (significant) influence on the second mode and, conversely, the first mode response does not depend upon K_2. For comparison, the open loop frequency response $G_{zd}(j\omega)$ (see also Fig. 13) is also included. It can be seen that in both loops, larger gains give more peak attenuation. However, increasing the gain also leads to the appearance of secondary peaks in the closed loop frequency response. These peaks arise from the interaction between the in-phase and quadrature components and thus, in view of Remark 2, one needs to use the TITO baseband or narrowband model to predict their occurrence. From Figs. 15 and 16, the choice

$$K_1 = K_2 = 1.5 \tag{12}$$

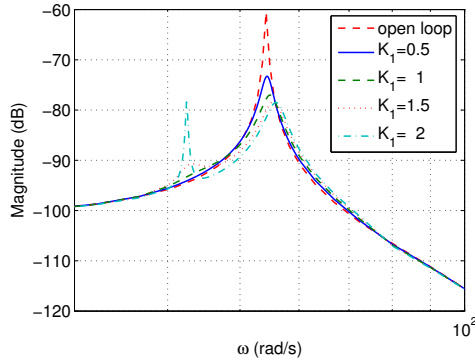appears to give a good compromise between peak attenuation and robustness.
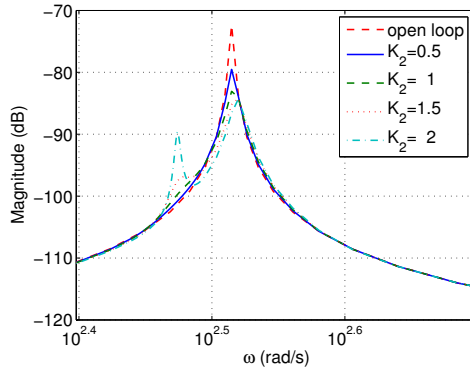

Fig. 15. Effect of K_1 on $T_{zd}(j\omega)$.

Fig. 16. Effect of K_2 on $T_{zd}(j\omega)$.

19

5.4 Closed Loop Results

Experimental frequency responses of the closed loop transfer function $T_{zd}(s)$ for several values of the controller gains were obtained. The low-pass filters $F_1(s)$ and $F_2(s)$ were taken as fourth order Butterworth filters as described in the previous section. We confirmed experimentally that there is little interaction between channels, so that the closed loop behaviour around ω_2 is essentially independent of K_1. Likewise, the closed loop behaviour around ω_1 is essentially independent of K_2. The results are documented in Tables 1 and 2. The tables contain the values of the peaks corresponding to the first two natural modes of the beam. It can be seen from these tables that more active control (i.e., larger gains) gives stronger peak attenuation, but decreases the stability margin of the closed loop. From the tables, it can also be seen that the experimentally determined critical gain for both loops is between 2 and 2.5. This agrees well with the critical gains predicted using the narrowband model in Section 5.3.

Fig. 17 shows the experimental frequency response when $K_1 = K_2 = 2$. The secondary peaks observed (using the narrowband model) in Section 5.3 are clearly visible in this figure.

Table 1
Effect of K_1 on peaks in $T_{zd}(j\omega)$ corresponding to ω_1.

K_1	peak value, dB
0	-53.77
0.25	-61.81
0.5	-66.06
1	-70.80
1.5	-72.99
2	-73.55
2.5	unstable loop

The experimental frequency response when $K_1 = K_2 = 1.5$ is shown in Fig. 18. As expected from the analysis in Section 5.3, this choice of controller gains does indeed give a good compromise between peak attenuation and robustness. It can be seen from Fig. 18 (see also Tables 1 and 2) that the resultant modulated and demodulated controller reduces the peak magnitudes of the oscillations by more than 19 dB (first mode) and 12 dB (second mode). This mitigation is accomplished with only small side-peak effects. Time domain analysis, such as the experimental step response contained in Fig. 19, confirm the quality of the design.

Table 2

Effect of K_2 on peaks in $T_{zd}(j\omega)$ corresponding to ω_2.

K_2	peak value, dB
0	-65.87
0.25	-70.14
0.5	-73.01
1	-76.25
1.5	-77.88
2	-78.56
2.5	unstable loop
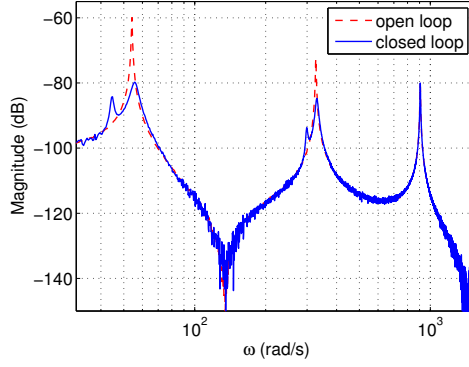
Fig. 17. Experimental frequency response with $K_1 = K_2 = 2$.
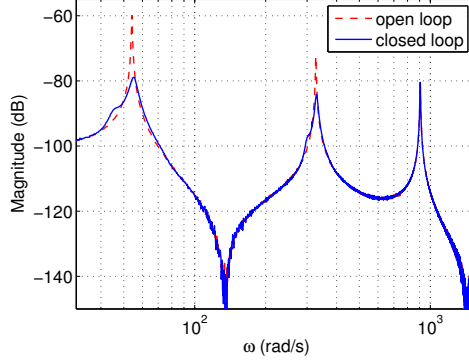
Fig. 18. Experimental frequency response with $K_1 = K_2 = 1.5$.

6 Conclusions

This paper has described the design of a controller based on modulation and demodulation principles aimed at the control of flexible structures. Both simulation and experimental results have been presented for a cantilever beam. These results confirm the efficacy of this approach. Insights into the design of the controller can be obtained by considering the SISO baseband model
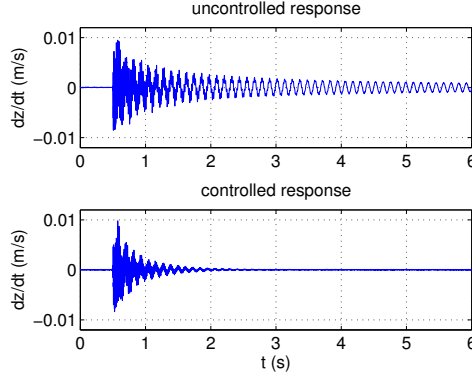
Fig. 19. Experimental step response of $\frac{dz}{dt}$, given $K_1 = K_2 = 1.5$.

which shows that the system is approximately describable as a first order model. However, to obtain greater precision one needs to consider the coupling between the quadrature and in-phase components. Both the TITO baseband model, which is approximate, and the narrowband model, which is exact, take these components into account. The narrowband model, in particular, has been shown to be capable of accurately predicting the performance/robustness trade-offs inherent in this controller architecture.

A   Proofs

A.1   Proof of Lemma 1

We provide a derivation for the transfer function from $U_{iI}(s)$ to $V_{iIf}(s)$. The other three transfer functions can be found in a similar manner. Suppose that $u_{iQ}(t) = 0$ and $\tilde{d}(t) = 0$. Then it is readily seen that $V_{iIf}(s)$ is given by

$$
V_{iIf}(s) = F_i(s)\left[G_m(s,\omega_i)U_{iI}(s) + \frac{1}{2}\left[e^{-j\phi_i}G(s+j\omega_i)U_{iI}(s+2j\omega_i)\right.\right.
$$
$$
\left.\left. + e^{+j\phi_i}G(s-j\omega_i)U_{iI}(s-2j\omega_i)\right]\right].
$$

We note that the bandwidth conditions on u_{iI} and $F_i(s)$ imply that $F_i(j\omega)U_{iI}(j\omega \pm 2j\omega_i) \approx 0$. Therefore, we can safely approximate $v_{iIf}(t)$ as

$$
v_{iIf}(t) \approx \mathscr{L}^{-1}\{U_{iI}(s)G_m(s,\omega_i)F_i(s)\}.
$$

It follows that the system from u_{iI} to v_{iIf} has an approximate transfer function given by $G_m(s,\omega_i)F_i(s)$.

A.2 Proof of Lemma 2

It can easily be seen that

$$U_{iI}(s) = \left[e^{-j\phi_i}V(s+j\omega_i) + e^{j\phi_i}V(s-j\omega_i)\right](FC)_i(s)$$

and that

$$2\tilde{U}_{iI}(s) = \left[e^{-j\phi_i}V(s) + e^{j\phi_i}V(s-2j\omega_i)\right](FC)_i(s-j\omega_i)$$
$$+ \left[e^{-j\phi_i}V(s+2j\omega_i) + e^{j\phi_i}V(s)\right](FC)_i(s+j\omega_i).$$

Similarly, we can show that

$$2\tilde{U}_{iQ}(s) = \left[e^{-j\phi_i}V(s) - e^{j\phi_i}V(s-2j\omega_i)\right](FC)_i(s-j\omega_i)$$
$$+ \left[-e^{-j\phi_i}V(s+2j\omega_i) + e^{j\phi_i}V(s)\right](FC)_i(s+j\omega_i).$$

As a consequence,

$$\frac{U(s)}{V(s)} = \left[e^{-j\phi_i}(FC)_i(s-j\omega_i) + e^{j\phi_i}(FC)_i(s+j\omega_i)\right],$$

from which the result follows.

References

Bode, H. W. (1945). *Network Analysis and Feedback Amplifier Design.* D. Van Nostrand Company, Inc.

Bodson, M., A. Sacks and P. Khosla (1994). Harmonic generation in adaptive feedforward cancellation schemes. *IEEE Trans. on Automatic Control* **39**(9), 1939–44.

Chang, T. N. (1993). Nonlinear tuning regulator for the control of lightly damped structures. In: *Proc. of the 1993 American Control Conference.* San Francisco, CA, USA. pp. 1503–1507.

Chen, Y. C., R. T. M'Closkey, T. Tran and B. Blaes (2005). A control and signal processing integrated circuit for the JPL-Boeing micromachined gyroscopes. *IEEE Trans. Contr. Syst. Technol.* **13**(2), 286–300.

Clark, R. L. (1997). Accounting for out-of-bandwidth modes in the assumed modes approach: Implications on collocated output feedback control. *ASME Journal of Dynamics, Measurement and Control* **119**(3), 390–395.

Clark, R. L., W. R. Saunders and G. P. Gibbs (1998). *Adaptive Structures Dynamics and Control.* Wiley. New York.

Corr, L. R. and W. W. Clark (2003). A novel semi-active multi-modal vibration control law for a piezoceramic actuator. *Trans. of the ASME J. Vibration and Acoustics* **125**(2), 214–222.

Fuller, C .R., S. J. Elliot and P. A. Nelson (1996). *Active Control of Vibration.* Academic Press. New York.

Gerber, M. A. (1978). Gravity gradiometry. Something new in inertial navigation. *Astronautics and Aeronautics* **16**(5), 18–26.

Goodwin, G. C., S. F. Graebe and M. E. Salgado (2001). *Control System Design.* Prentice-Hall.

Hagood, N. W. and A. von Flotov (1991). Damping of structural vibrations with piezoelectric materials and passive electrical devices. *J. Sound Vibr.* **146**(2), 243–268.

Hagood, N. W., W. H. Chung and A. von Flotov (1990). Modeling of damping of piezoelectric actuator dynamics for active structural control. *J. Intell. Material Syst. Structures* **1**(3), 327–354.

Lau, K., D. E. Quevedo, G. C. Goodwin and S. O. R. Moheimani (2004*a*). Multi-modal modulated and demodulated vibration control of flexible structures using piezoelectric transducers. In: *3rd IFAC Symposium on Mechatronic Systems, Sydney, Australia, Sep. 6-8, 2004.*

Lau, K., G. C. Goodwin and R. T. M'Closkey (2004*b*). Fundamental performance limitations of modulated and demodulated systems. In: *Proc. 2004 American Control Conference, Boston, MA, USA, Jun. 30 - Jul. 2 2004.*

Lazarus, K. B., E. F. Crawley and J. D. Bohlman (1991). Static aeroelastic control using strained actuated adaptive structures. *J. Intell. Material Syst. Structures* **2**(3), 386–440.

Leland, R. P. (2001). Adaptive tuning for vibrational gyroscopes. In: *Proc. 40th IEEE Conf. on Decision and Control, Orlando, FL, USA, Dec. 4-7, 2001.* pp. 3447–52.

Moheimani, S. O. R. (2000). Experimental verification of the corrected transfer function of a piezoelectric laminate beam. *IEEE Trans. Contr. Syst. Technol.* **8**(4), 660–666.

Moheimani, S. O. R. (2003). A survey of recent innovations in vibration damping and control using shunted piezoelectric transducers. *IEEE Trans. Contr. Syst. Technol.* **11**(4), 482–494.

Moheimani, S. O. R., A. J. Fleming and S. Behrens (2001). A highly resonant controller for piezoelectric shunt damping. *Electron. Lett.* **37**(25), 1505–1506.

Moheimani, S. O. R. and G. C. Goodwin (2001). Guest editorial: Introduction to the special issue on dynamics and control of smart structures. *IEEE Trans. Contr. Syst. Technol.* **9**(1), 3–4.

Moheimani, S. O. R., D. Halim and A. J. Fleming (2003). *Spatial Control of Vibration: Theory and Experiments.* World Scientific. Singapore.

Pota, H. R., S. O. R. Moheimani and M. Smith (1999). Resonant controllers for flexible structures. In: *Proc. 38th IEEE Conf. on Decision and Control, Phoenix, AZ, USA, Dec. 7-10 1999.* pp. 631–636.

Serón, M. M., J. H. Braslavsky and G. C. Goodwin (1997). *Fundamental Limitations in Filtering and Control.* Springer-Verlag, London.

Vaidyanathan, P. P. (1993). *Multirate Systems and Filter Banks.* Prentice-Hall.

Englewood Cliffs, New Jersey.